Received: 8 November 2024 | Revised: 17 December 2024 | Accepted: 27 December 2024

DOI: 10.1002/pc.29467

RESEARCH ARTICLE

Polymer COMPOSITES WILEY

Improvement of thermal, electrical, and tribological performances of GnPs composites produced by selective laser sintering

E. Mingione[1] | D. Salvi[2] | D. Almonti[2] | G. S. Ponticelli[3]

[1]Department of Economics, Engineering, Society, and Business Organization, University of Tuscia, Viterbo, Italy

[2]Department of Enterprise Engineering, University of Rome Tor Vergata, Rome, Italy

[3]Department of Engineering, University Niccolò Cusano, Rome, Italy

Correspondence
E. Mingione, Department of Economics, Engineering, Society, and Business Organization, University of Tuscia, Via del Paradiso, 47, 01100, Viterbo, Italy.
Email: emanuele.mingione@unitus.it

Abstract

In the present work, Graphite nanoPlatelets/Polyamide-12 (GnPs/PA-12) particle composites were produced through additive manufacturing (AM). The selective laser sintering (SLS) technology was used to manufacture 3D-printed composite components by means of a powder mix of GnPs and PA-12. The analyzed combination of technology and materials allows to obtain parts with improved thermal, electrical, and tribological properties, while maintaining a low production cost. In total were realized 5 different scenarios, each one with a different wt% of the GnPs reinforcement (2-4-6-8-10 wt%), and compared the results to the PA-12 matrix. Experimental tests were performed to study the morphology (profilometry, SEM, wettability), the electrical conductivity under different normal loads (0.1–1 kN), the thermal performance, and the tribological properties of each sample. The results show that the increase of GnPs particles dispersed in the matrix leads to a hydrophobic behavior of the surface. An improvement in electrical conductivity (from 10^{-11} S/cm of the pure PA-12 matrix to 10^{-4} S/cm of the 10 wt% GnPs) and thermal performance (33,6% improvement for the best-case scenario compared to the bare matrix) was observed. Tribological tests underlined a reduction of 25% in friction coefficient and an improvement of 80% in wear resistance compared to the PA-12 matrix.

Highlights

- 3D printed GnPs/PA-12 composites does not exhibit any significant geometrical alteration.
- GnPs enable hydrophobic surfaces with increased contact angles.
- Electrical conductivity improved from 10^{-11} S/cm of the unfilled PA-12 matrix up to 10^{-4} S/cm, for the 10 wt% GnPs sample.
- Thermal performance improves up to 33.6% with GnPs reinforcement.
- 10 wt% GnPs reduces friction by 25% and wear by 81%.

KEYWORDS

additive manufacturing, GnPs, PA-12, particle composites, PBF-LB/P, SLS

1 | INTRODUCTION

The advantages of additive manufacturing (AM) combined with the mechanical and functional features of polymer matrix composites have drawn intense research interest recently.[1,2] Among the different AM techniques that process polymers, Laser-Based Powder Bed Fusion (PBF-LB/P) commonly known as selective laser sintering (SLS), is considered particularly promising due to the near-isotropy of the components produced, the total lack of support structures,[3] the easy accessibility to novel materials,[4,5] including composites,[6,7] thus opening for a direct end product fabrication without the need for subsequent post-processing.[8,9]

Because of their great specific strength, flexibility, high processability, and corrosion resistance, polymers are a valuable class of materials in engineering. However, most polymers are by nature nonconductive materials both thermally and electrically, and very often, they have limited mechanical properties, like stiffness, tensile strength and wear resistance.[10,11] Among polymers, polyamide 12 (PA-12) is a widely used engineering material for SLS, thanks to its excellent thermal stability, good impact strength, good fracture resistance, and high processability,[12] experiencing great interest, especially from the automotive and aerospace industries.[13,14] However, significant efforts have been made so far to further increase the qualities of polymer-based parts by the application of functional reinforcements[15,16] since these sectors require to satisfy stringed regulations, with the aim to obtain a material with improved stiffness and toughness,[17] specific electrical and thermal properties,[18,19] possibility to realize complex shapes that are impractical to produce using traditional techniques,[20] lightweight structures,[21] low-friction[22,23] and wear-resistant features,[24,25] and chemically stable.[26]

Carbon-based nanofillers, for example, graphene nanoplatelets, carbon nanotubes, carbon black, and so forth, are frequently employed as functional and reinforcing fillers for polymers to modify their characteristics both in SLS[27] and fused filament fabrication.[28] Carbon nanofibers (CFs) and graphene nanoplatelets are usually chosen over carbon-based nanofillers because of their strong Van der Waals affinity, preventing agglomeration during mixing,[1] and save material costs since they can be made using a scalable production method.[29] Moreover, nano-scale particle fillers offer the advantages of having larger surface areas for stress transfer from the polymeric matrix to the particles and require smaller loadings.[3]

The use of the SLS technique to process composite powders obtained through the incorporation of strong and highly conductive carbon-based reinforcements into the polymeric matrix can provide, in this context, a suitable solution able to fulfill the mentioned requirements for functional applications. Several attempts have been made to improve the characteristics of PA-12 by incorporating carbon-based fillers for SLS processing. Lopes et al.[30] prepared PA-12/GnP samples by using a mechanically mixed composite powder with various weight percentages of reinforcement, between 0.5 and 3. Despite the decrease in mechanical properties, they demonstrated an improvement of the electrical conductivity up to 10^{-6} S/cm. These results were then confirmed by Lupone et al.,[1] who laser sintered hybrid composite powders made of PA-12/CF and PA-12/CF/graphite by mechanical mixing of various weight percentages of fillers, up to 20%. They declare that although the addition of CFs improves the mechanical properties of neat PA-12, further mixing with graphite deteriorates the performances, especially at higher weight percentages. While, at the same high percentages of fillers, the electrical conductivity reaches values between 10^{-4} and 10^{-5} S/cm, against 10^{-11} S/cm of the unfilled PA-12. Unlike the previous works, Meng et al.[10] propose a novel approach for PA-12/GnP powder mixing based on electrostatic self-assembly to obtain controlled weight compositions at 0.1%, 0.2%, and 1%. However, they also state that only at the highest concentration of Graphite Nanoplatelets (GnPs) electrical and thermal conductivities increase, up to 10^{-5} S/cm and 0.41 W/m K respectively, against 10^{-11} S/cm and 0.19 W/m K of the base material, while demoting the mechanical properties. Badini et al.[31] tested commercial composite powders with a much greater CF weight concentration, of about 19% and 28%, highlighting that the orientation of the fillers plays a crucial role in the final mechanical properties with a detrimental effect when the fibers are oriented perpendicularly to the applied load, as further verified by Khudiakova et al.[32] They performed a systematic analysis on PA-12/CF composite samples obtained through mechanical mixing of commercial powders with a weight percentage of 12% of filler, underlining the importance to optimize fiber orientation in essential and critical parts. Chen et al.[33] report on the adoption of a PVA intermediate medium for the adhesion of GnPs on PA-12 particles, with weight concentrations of 0.1% and 1%. While at lower concentrations the PA-12/PVA/GnP composite samples exhibited a modest improvement in mechanical properties, these were deteriorated by increasing the weight percentage of GnPs. Gadelmoula and Aldahash[25] adopted an in-house developed PA-12/CF/GnP composite powder made of 5% and 2% in weight of CF and GnP respectively. In contrast with the described behavior of the mechanical properties at increasing concentrations of carbon-based reinforcements, they state that the tribological properties, that is, steady-state coefficient of friction, contact temperature, and wear pattern, are independent from orientation.

From the literature analysis, there is a large number of combinations of filler-polyamide powders, mixing

processes, and fabrication parameters currently being studied to find the optimal components to satisfy the stringent requirements of the modern automotive and aerospace industries. Moreover, the GnPs reinforcement is a well-balanced trade-off between the increase in performance and the material cost compared to a pristine Graphene reinforcement. However, despite the promising features of the PA-12/carbon-based composite powders processed through SLS, further research is needed to explore and understand the mechanical, electrical, thermal, and tribological properties under a wide range of operating conditions. In this context, the present study attempts to fill the lack of adequate thermo-electric characterization of this type of composites in the scientific literature and allows the manufacturing of PA-12/GnPs composites at different weight percentages obtained through mechanical mixing and processed by using a commercial SLS machine, which could be industrially relevant due to the cheapness of the reinforcement used and the mixing methodology. The produced samples were tested to identify the morphological, electrical, thermal, and tribological properties, in order to understand the effect of the filler content on the resulting performances.

2 | MATERIALS AND METHODS

Graphite Nanoplatelets powder used in these experiments was supplied by Nanesa S.r.l (Via Calcutta, 8, Rome, Italy). and the physical properties are indicated in Table 1, while Polyamide 12 powder (PA-12 smooth commercial powder) was supplied by the company Sinterit (Nad Drwiną 10/bud. B3, Kraków, Poland) and employed as the polymeric matrix for the nanocomposite.

Graphite Nanoplatelets were mixed with PA-12 powder by mechanical mixing. Respectively different weights of GnPs (2, 4, 6, 8, and 10 wt%) were dispersed into the matrix powder by means of a roto-vibrational sieve. To guarantee the homogeneity of the mixture, the process was repeated 10 times. Afterward, the mixture was dried in a static oven at a temperature of 80 °C for 24 h.

Since the realized powder mixtures are not commercial, is interesting to evaluate the flowability. In particular, the flowability has been evaluated with the Hausner ratio (HR) calculated with the following equation.[34,35]

$$HR = \rho_{tap}/\rho_{bulk} \quad (1)$$

where ρ_{tap} is the density of the mixture calculated after the densification of the powder, and ρ_{bulk} is the bulk density. The densities are determined by demarcating a small cuvette with known volumes, then inserting a small mass of powder into the cuvette to determine the bulk density

TABLE 1 Physical properties of the GnPs reinforcement used as declared by the producer.

Features	Content	Units
Graphite Type	Graphite Nanoplatelets	–
Carbon content	>97	[wt%]
C:O ratio	44:1	–
Bulk density	0.20–0.42	[g/cm^3]
Specific surface area	30	[m^2/g]
Average particle lateral size – D90	30	[μm]
Average particle lateral size – D50	25	[μm]
Average thickness	14	[nm]

and gently tapping it vertically against a padded bench top 50 times to calculate the tapped density.[36] The process was repeated 3 times to ensure the repeatability of the results obtained.

Before printing, the powder mixtures were analyzed by using Differential Scanning Calorimetry (DSC) to evaluate if any change in the sintering window occurred due to the addition of GnPs. This is the temperature interval between the melting point (T_M) and the recrystallization (T_R) of the polymer and represents that range where the bed temperature of a semi-crystalline polymer is typically fixed to keep it there long enough to reduce the adverse effects of thermal stress following consolidation.[2] To this end, the tests were conducted using the DSC Q2000 by TA Instruments (159 Lukens Dr., New Castle) and the results were analyzed by means of the software TRIOS. It was set a heating/cooling speed of 10 °C/min, a nitrogen flow of 20 mL/min, and a temperature interval between 20 and 225 °C, carried out in one complete cycle of heating/cooling per condition. The background correction was performed by doing an empty crucible run in which was evaluated the heat flow associated with the empty crucible and afterward, the reference baseline obtained from that run was subtracted from the sample heat flow data.

Selective laser sintering process was employed to 3D-print neat polyamide and its GnPs reinforcement at the indicated GnPs weight concentrations. The schematic of the process is presented in Figure 1A.

The sample geometry consists of 30 × 30 × 3 mm^3 square plate, which was used for all the subsequent characterization tests. The SLS machine used to produce the samples was the Lisa Pro by Sinterit (Nad Drwiną 10/bud. B3, Kraków, Poland). It is equipped with an IR laser diode type at a wavelength of 808 nm and power up to 5 W. During the 6 different 3D printing processes

(each one with a different GnPs wt% concentration), the layer thickness and the chamber temperature were kept constant respectively at 0.125 mm and 200 °C, the samples were all printed in the XY plane. After the 3D printing process, the samples were sandblasted with aluminium oxide by Smyris Abrasivi S.r.l. (Via R. Sanzio, 9, Pero, Italy) characterized with 1.2 μm average diameter and a shape factor of 0.67, at a pressure of 2 bar and an angle of about 60° for 30 s to remove the excess of powder on the surface. The final produced samples at different wt% are shown in Figure 1B. In total were produced 6 different wt% of GnPs reinforcement scenarios and replicated 3 times, for a total of 18 samples, which were tested for all the characterizations.

After the production phase, a density evaluation of the different specimens was performed to assess the differences between theoretical values and measured ones. The theoretical density values were obtained by the mixture rule, following the equation:

$$\rho_c^t = \frac{1}{\frac{W_m}{\rho_m} + \frac{W_r}{\rho_r}} \quad (2)$$

where ρ_c^t represents the density of the composite, W_m and ρ_m the weight fraction and density of the PA12 matrix, W_r and ρ_r the weight fraction and density of the GnP reinforcement. The measured density values were calculated considering the volume of the samples and weighting specimens by means of the analytic scale Sartorius BCE ENTRIS II Serie, by Sinergica Soluzioni S.r.l. (Viale Luca Gaurico, 9, Rome, Italy).

Successively, each one was morphologically characterized, to verify if the addition of the reinforcement significantly altered the specimens' surface features. The analysis was performed by using the 3D surface profiling system Talysurf CLI 2000 by Taylor Hobson (2 New Star Road, Leicester, United Kingdom) to collect roughness profiles. For each sample, a total of 15 profiles with 12.5 mm length, an interspace of 100 μm, and a resolution of 1 μm were collected, according to the ISO 4287 standard. The roughness of the treated samples was studied considering the Roughness Average (Ra) and 10 Point Height of Irregularities (Rz). The profiles were then elaborated by means of surface analysis software Mountains v.8.0 by Digital Surf (16 rue Lavoisier, Besançon, France), which collected Ra and Rz using a 2.5 mm Gaussian Filter.

To evaluate the homogeneous dispersion and adhesion of the reinforcement within the matrix, a scanning electron microscope (SEM) analysis was performed by means of the SNE ALPHA produced by SEC Co. Ltd. (111 Saneop-ro, Gwonseon-gu, Suwon-si, Gyeonggi-do, South Korea). Before the observation, to increase the

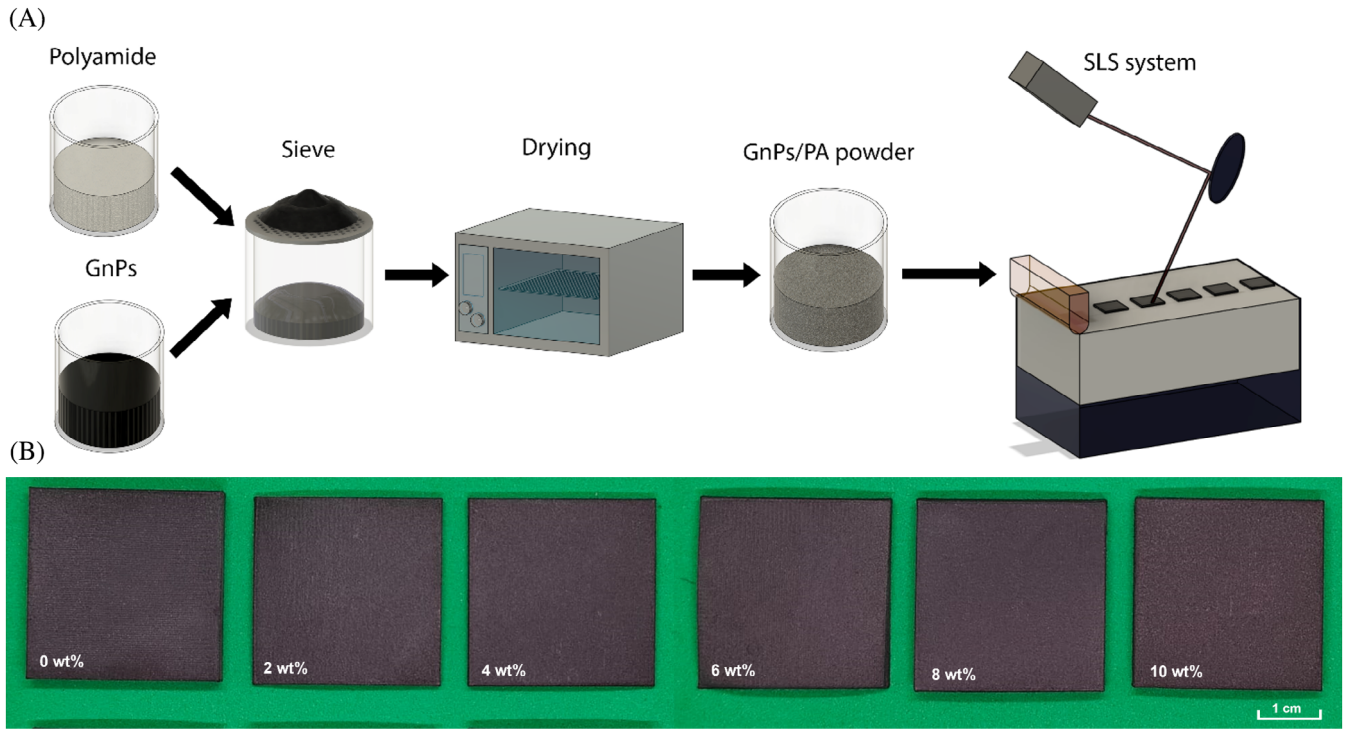

FIGURE 1 (A) Schematic of the production process of the samples (B) GnPs/PA-12 reinforced samples realized through the 3D printing process.

quality of the images, the samples were coated with platinum for 5 min with an ion sputterer MCM-100 by SEC Co. Ltd. Afterward, images were acquired both on the external surface and in the cross-section to assess for homogeneous reinforcement presence with a 20 kV operating voltage at several magnifications.

Since the GnPs are notoriously, highly hydrophobic[37] wettability tests were performed to evaluate wetting angle and water absorption differences in each scenario. The analysis was performed by means of BIOLINS SCIENTIFIC Attension Theta Flow instrument (Hängpilsgatan 7, Västra Frölunda, Sweden) using a deionized water droplet with a volume of 5 μL. Test duration time was 60s and the data acquisition rate was set at 2.5 FPS in order to obtain 150 frames.

Since the auto-lubricating properties of the GnPs are widely known in literature,[38] to evaluate the improvement in tribological performances (friction coefficient, wear resistance) of the produced composites, tribological tests were carried out using a standard tribometer by CSM Instruments (Rue de la Gare 4, Peseux, Switzerland), in the ball-on-flat configuration with a half-amplitude of 2.5 mm and a maximum speed of 5 cm/s. The tests were repeated 3 times to assess the repeatability of the results, and carried out with a normal load of 2 N[39] using an Al_2O_3 ceramic ball with a diameter of 6 mm within a sliding distance set at 200 m. This load, considering the counterpart diameter used, the Young modulus of the coupled materials (350,000 MPa for Al_2O_3, 1470 MPa for the PA12 smooth) and their Poisson modulus (0.3 for Al_2O_3 and 0.45 for PA12 smooth), develop a maximum Hertzian contact pressure of 40 MPa, compatible with the application of low-friction polymer gears proposed by Li et al.[40] To evaluate the wear resistance, 3D maps of the wear track (5.5×1.2 mm^2 with a spacing of 2 μm in both directions) were collected using the aforementioned 3D profilometer. Wear volumes were calculated once the maps were acquired by means of the surface analysis software Mountains v.8.0.

GnP is known to have excellent electrical and thermal properties (thermal conductivity of ~4000 $Wm^{-1}K^{-1}$, electrical conductivity of $\sim 1.5 \times 10^6$ S/m),[41] and many researchers used it as a reinforcement to improve the thermo-electrical properties of non-conductive matrixes[42] including PA-12.[10] For this reason, the electrical conductivity and thermal performance of each different wt% sample were evaluated to verify whether the addition of the GnPs reinforcement turns the composite into a fairly thermo-electrically conductive material. First, the electrical resistance of the samples was measured by means of a resistance meter DC series 2840 by B&K Precision (22,820 Savi Ranch Pkwy, Yorba Linda, California, United States) using Kelvin test leads with a 4-point probe configuration. Since the samples produced through SLS are notoriously porous[3] it was investigated the influence of an external compressive load since a porosity closure brings the GnPs closer together, which may affect the electrical resistivity of the material. With this aim, the tests were performed by applying a fixed compressive load with the MTS Insight 5 by MTS S.r.l. (Strada Pianezza 289, Torino, Italy) with a load cell of 5 kN to assess the influence of an external force on the electrical behavior. For this purpose, 10 different loads ranging from 0.1 to 1 kN were investigated. The schematic of the test is shown in Figure 2A.

After the test, the electrical conductivity of the samples is calculated through the following equations:

$$\rho = \frac{R \cdot A}{l} [\Omega \cdot cm] \tag{3}$$

$$\sigma = \frac{1}{\rho} [S/cm] \tag{4}$$

where σ is the electrical conductivity, ρ is the resistivity, R is the measured electrical resistance, A the cross-sectional area of the samples and l is the sample's thickness.

To evaluate the improvement in thermal performance, a comparative test between the produced samples, schematized in Figure 2B, was conducted by means of a thermal imager Fotric 348A by Fotric (17,250 Dallas Pkwy, Dallas, Texas, United States) that has a thermal sensitivity of 30 mK in the range −20 up to 120 °C. First, the specimens were laid down on a hot plate set at a temperature of 45 °C for 60 min in order to initialize the test temperature for each specimen around the same temperature value as shown in Figure 2B. Subsequently, the hot plate was heated up to a set temperature of 100 °C and the thermal history of the samples was recorded with the IR camera at a distance of 600 mm and by imposing an emissivity of 0.85 which is both the mean value for PA12 and GnPs.[43] The results analyzed by means of the thermal imager software Analyzers with a data acquisition rate of 2 FPS for 700 s. In particular, the history of average temperature in the whole area and the central spot of each sample were recorded during the test. To evaluate the improvement in the thermal behavior, it was also calculated the time to reach 90 °C for each wt% considered.

3 | RESULTS AND DISCUSSION

The flowability results are shown in Table 2. According to the literature,[44] an HR below 1.25 suggests free-flowing powder, while an HR above 1.4 indicates potential fluidization

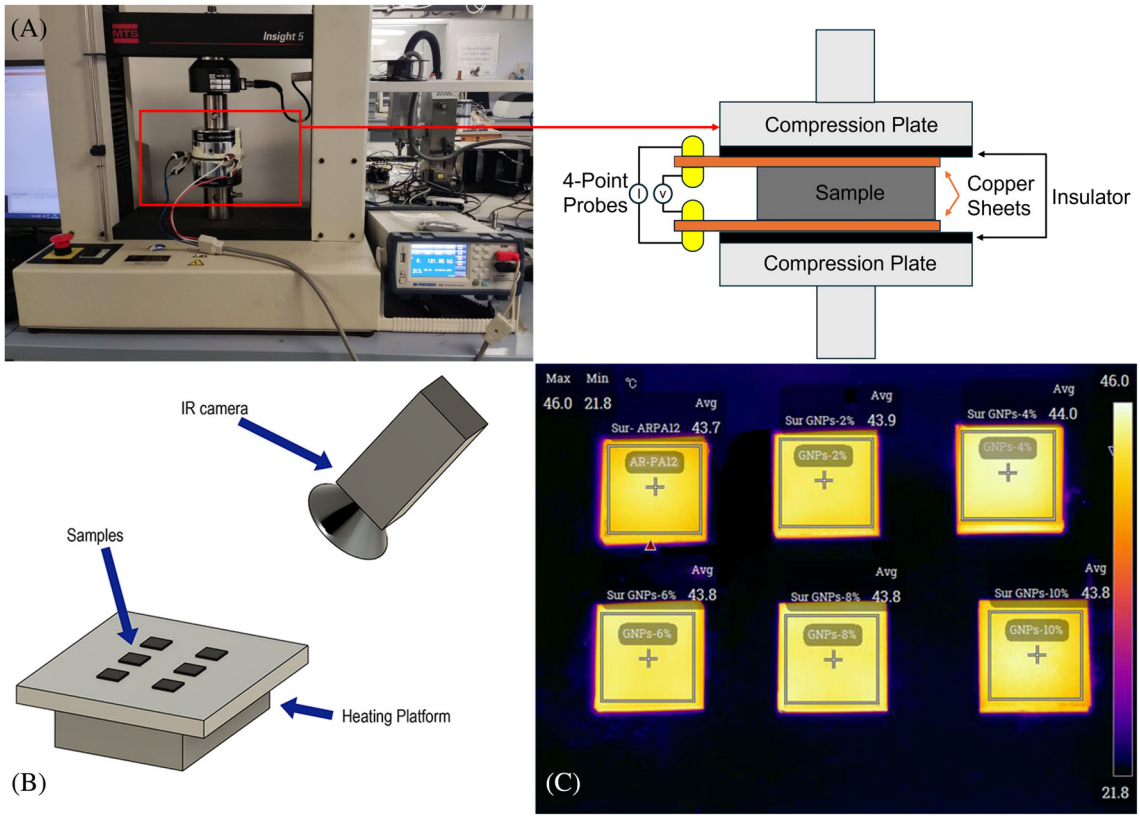

FIGURE 2 (A) Schematic of the experimental setup for electrical conductivity tests; (B) Schematic of the experimental setup for thermal tests; (C) Thermal image of the specimens at the beginning of the thermal test.

GnP [wt%]	HR	T_M [°C]	T_R [°C]	ρ_c^t [g/cm^3]	ρ_c^e [g/cm^3]
0	1.16 ± 0.01	180.65	155.56	0.968	0.968 ± 0.019
2	1.14 ± 0.02	180.32	155.66	0.899	0.889 ± 0.024
4	1.13 ± 0.02	178.99	155.95	0.864	0.848 ± 0.037
6	1.13 ± 0.02	180.35	156.17	0.831	0.806 ± 0.043
8	1.12 ± 0.02	180.35	156.18	0.801	0.717 ± 0.043
10	1.12 ± 0.02	180.53	156.18	0.773	0.664 ± 0.054

TABLE 2 Hausener ratio (HR) values, Melting (T_M) and recrystallization (T_R) temperatures evaluated through the analysis of the DSC diagrams, and theoretical (ρ_c^t) and experimental (ρ_c^e) density calculations, for the various wt% samples.

issues due to cohesive properties. For all the analyzed powder mixtures, the HR is lower than 1.25, which assures the free-flowing powder status. In particular, the HR slightly decreases as the wt% of reinforcement increases, due to the comparable particle sizes in two directions between the PA12 powder (Mean particle size 38 μm) and GnPs (Mean plane particle size 30 μm). The enhanced flowability is attributable to the small thickness of the GnPs in the third dimension (14 nm), enabling to infiltrate the gaps left by the polymeric powder.

The experimental campaign involved a preliminary investigation to evaluate the sintering window of the various PA-12/GnP mixtures by DSC to define the optimal process parameters to fabricate the sample needed for characterization. In Appendix A are shown the sintering intervals as the temperature range between the melting point and the recrystallization of the material powder, while the melting and recrystallization temperatures are presented in Table 2. The addition of GnPs can affect the sintering window due to the shift of the recrystallization to higher temperatures, which can be attributed to the nucleating effect of the GnPs that prevents the mobility of polymer chains.[45,46] However, in this case, the reduction of the sintering window extent is negligible and the same process parameters will be adopted to fabricate the sample at different GnPs weight concentrations.

Table 2 also reports the theoretical density calculated using the rule of mixtures (ρ_c^t) and the experimental density (ρ_c^e) measured on the samples as the wt% concentration of GnPs varies. It can be seen that in the case of the

TABLE 3 Roughness results of the produced samples with different reinforcement concentrations (wt%). Avg. is the mean value, while St. Dev. is the standard deviation.

GnP Concentration [wt%]	Ra [μm]		Rz [μm]	
	Avg.	St. Dev.	Avg.	St. Dev.
0	10.29	0.55	66.87	3.42
2	10.64	0.77	69.21	4.73
4	10.67	0.58	68.52	5.08
6	9.90	0.48	61.81	4.24
8	9.95	0.48	64.78	3.85
10	10.84	0.42	69.54	4.82

bare PA-12 sample, the theoretical value is perfectly comparable to the experimental one. As a result of the low density of the reinforcement, the addition of GnPs leads to a significant reduction in density. It is interesting to note that the measured density is lower than the theoretical one in each scenario with GnPs. In particular, it is observable that the gap between the two values becomes larger as the amount of GnPs in the compound increases. This effect can be attributed to the microporosities of the components, which become more pronounced as the amount of GnPs increases, due to the thermal inertia of GnPs, which inhibits the complete sintering of the polymer powder around the particles.

3.1 | Surface analysis

In this paragraph are illustrated the morphological results obtained through the roughness measurements, the SEM acquisition, and the wettability tests as discussed in the previous section. The main roughness results are shown in Table 3.

The analysis did not reveal any noticeable difference between the samples, in fact, considering the mean value and standard deviation of any GnPs concentration, every other scenario turns out to be within that band. This result suggests that the inclusion of the GnPs in the PA-12 matrix did not significantly alter the surface quality of the specimens, without impacting the SLS production process.

To confirm the previous assumption, a surface analysis through SEM was performed. In particular, as shown in Figure 3, the GnPs reinforcement seems to be homogenously included (circled in red) without altering the surface quality even at the highest wt%. No pores or vacancies can be observed in the zone near the GnPs platelets on the external surface, which is printed within a single layer on the XY plane, suggesting that during the production process, there is no interaction between the laser beam and the reinforcement in the considered direction. This result can be attributable to the inertness of the GnPs and their capacity to withstand high temperatures.[47]

To verify that the GnPs are evenly dispersed all over the matrix, SEM images of the specimens' cross-sections were examined. From Figure 4 it is notable that a higher quantity of well-adhered GnPs reinforcement, highlighted also by the flakes-like shape which is more and more present at the increase of the wt% concentration. However, in contrast to what was noticed on the surface (XY plane) since the cross-section was taken on the XZ plane, there is an increase in porosity and the presence of partial sinterization on zones adjacent to the GnPs flakes as the reinforcement concentration increases. The former increase in porosity is likely caused by the thermal inertia of the reinforcement, in particular, the increase when the GnP flake is present within a layer, there will be no physical continuity within the PA-12 matrix of the subsequent layer due to the different chemical affinity between the polymer and the reinforcement, resulting in a porosity in that intralayer zone. The latter partial sinterization presence can be attributed to the thermal barrier effect, consistent with the study of Cilento et al.,[48] of the GnPs flakes nearby a particle of PA-12 matrix, which leads to a reduction of the local temperature, which will be not sufficient for the sinterization of the particle. The detail of the GnPs flake both on the surface and cross-section for the 10 wt% sample is shown in Figure 5. In particular, in Figure 5A it is possible to observe the flakes randomly distributed among the surface, while Figure 5B highlights the good adhesion of the reinforcement branched all over the matrix and the presence of not sintered PA-12 particles.

The results obtained from the wettability tests are summarized in Figure 6. In particular, Figure 6A shows the wetting angle variation during the acquisition time of 60 s. From the plots is noticeable a considerable difference in the contact angle (the angle of the droplet at the start of the test), which confirmed the hydrophobic behavior of the GnPs, since a higher quantity in wt% present in the matrix, results in a higher contact angle. Moreover, can be also observed a reduction in the slope of the wettability angle over time, indicative of a reduction in the absorption capacity of the surface. This behavior is attributable to the presence of the GnPs flakes that

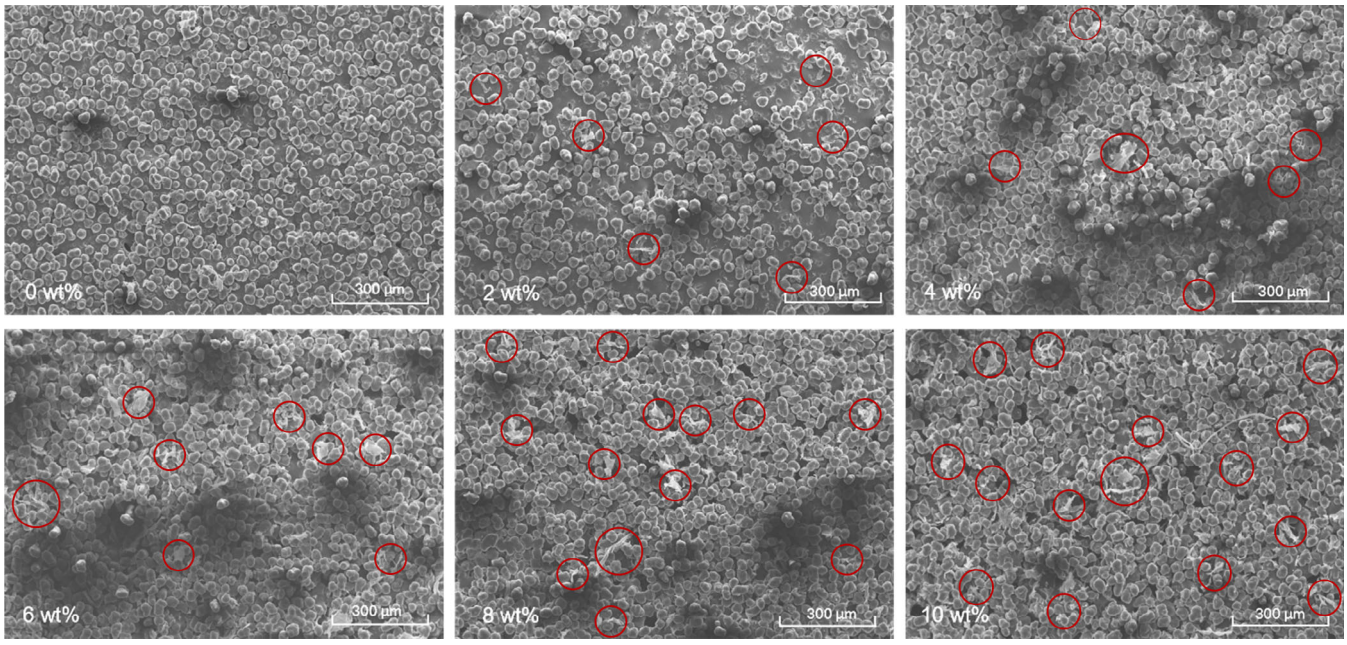

FIGURE 3 External surface SEM images of the different GnPs wt% specimens at ×250 MAG, circled in red the presence of the GnPs reinforcement embedded in the matrix.

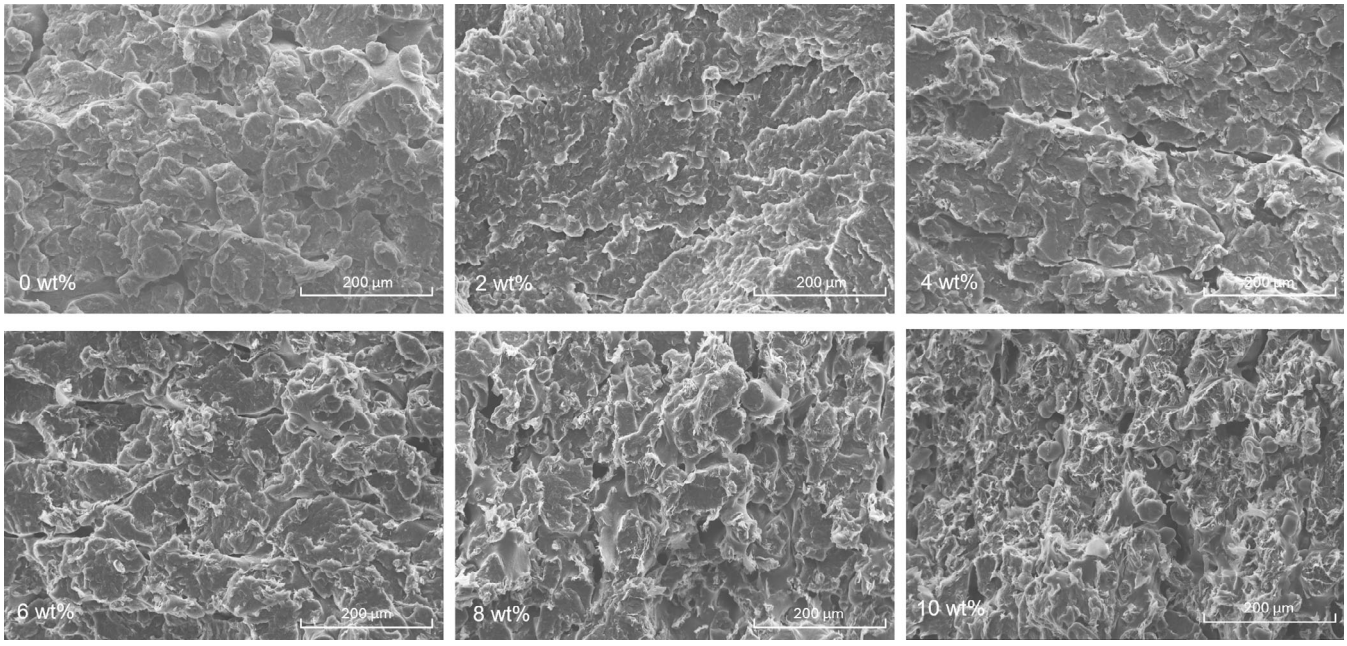

FIGURE 4 Cross-section SEM images of the samples with different GnPs wt% at ×500 MAG.

isolate the water droplet inhibiting the absorption of the droplet by the underlying porous surface.[49] In Figure 6B,C are shown the values of the contact angle of the best and worst case (respectively 10 and 0 wt%). The hydrophobic behavior of the surface is widely improved by a 43% increase in the contact angle, passing from a hydrophilic (<90°) to a hydrophobic (>90°) behavior.

3.2 | Electrical and thermal characterization

The plots of electrical conductivity for the different wt% samples at various external forces are shown in Figure 7 (electrical conductivity presented in logarithmic scale). The 0–2 wt% plots are missing because the instrumentation used

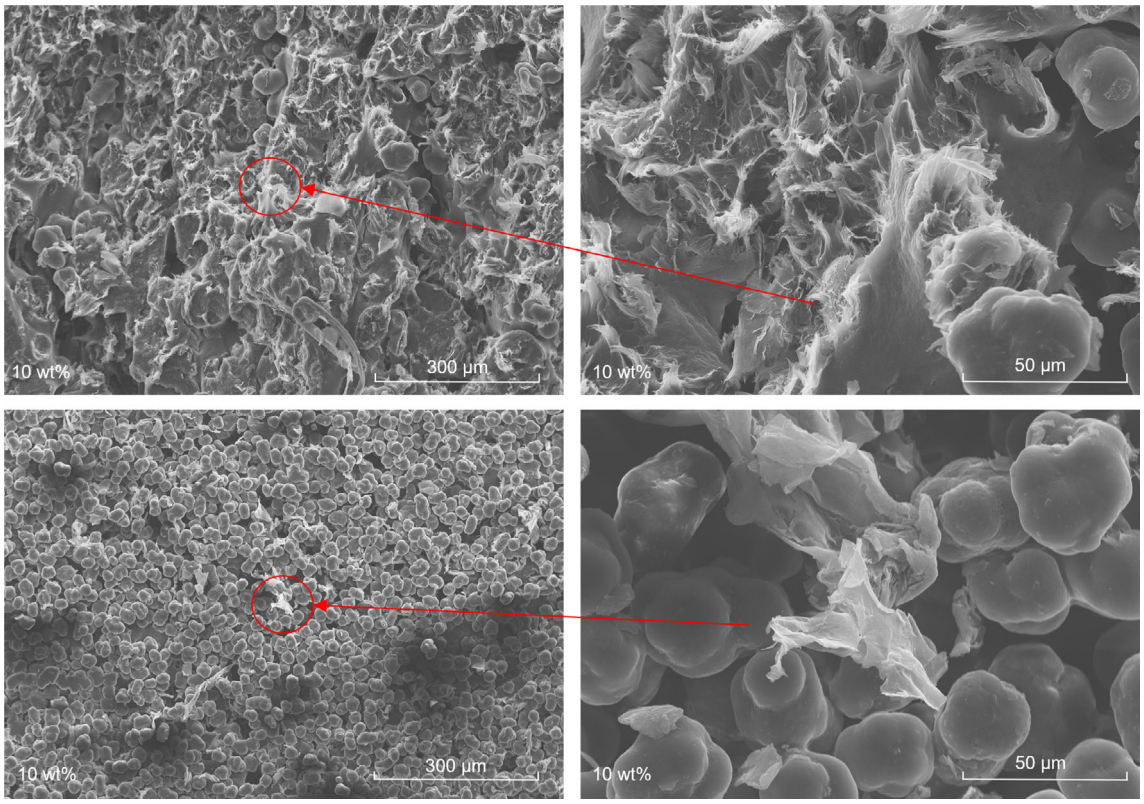

FIGURE 5 Details of the GnPs presence in the 10 wt% sample: (A) external surface at ×250 and ×2000 MAG; (B) cross-section at ×250 and ×2000 MAG.

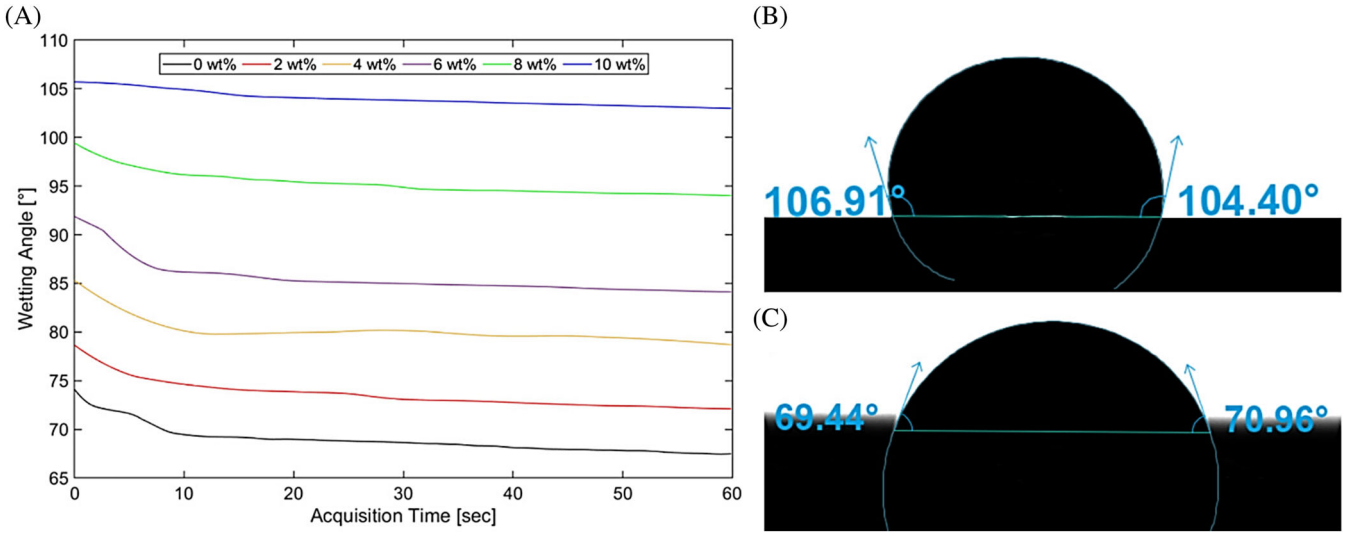

FIGURE 6 (A) Wetting angle of the samples at different GnPs wt% over acquisition time; (B) Contact angle of the GnPs 10 wt% specimen after 10 s (25 frames); (C) Contact angle of the GnPs 0 wt% specimen after 10 s (25 frames).

was not able to detect the electrical resistance (the upper limit is 99.99 MΩ) which means that the samples can be referred to as an electrical insulator. The measured average and standard deviation values for the electrical tests are shown in Appendix A to improve the readability of the results. From the plots, the most striking result to emerge is that the 4 wt% GnPs dispersion is the percolation threshold for electrical conductivity, with average values between $3.87 \cdot 10^{-10}$ S/cm at the lowest load of 100 N and $1.07 \cdot 10^{-9}$ S/cm at the highest load of 1000 N, values for which the material can be considered weakly conductive. For the 6 wt% samples, there is an increase of two order of

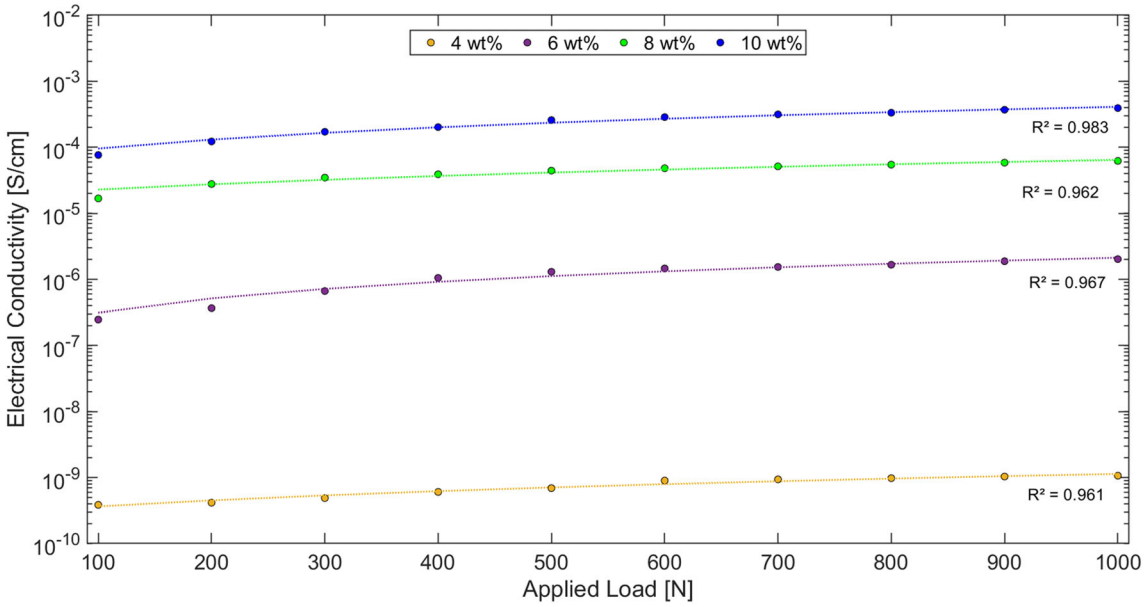

FIGURE 7 Plots of electrical conductivity versus applied load of the different wt% samples (0–2 wt% samples are not included since the electrical conductivity could not be measured with the experimental setup used).

magnitude of the measured electrical conductivity ranging from a $2.48{\cdot}10^{-7}$ to $2.02{\cdot}10^{-6}$ S/cm (comparable with the electrical conductivity of the silicon, which is a semiconductor),[50] while for the 8–10 wt% of GnPs reinforcement, the electrical conductivity raises up of 2 more order of magnitudes, varying within the range $1.68{\cdot}10^{-5}$–$6.22{\cdot}10^{-5}$ S/cm for the 8 wt% sample (comparable with the electrical conductivity of the Boron[51]), and a value from $7.64{\cdot}10^{-5}$ to $3.93{\cdot}10^{-4}$ S/cm for the 10 wt% sample (comparable with the Germanium).[52] Considering the initial condition of the PA-12 matrix, there was a total increase of more than 8 orders of magnitude in the electrical conductivity for the highest wt% sample. It is also notable that, the electrical conductivity increases linearly as the applied load increases for all kinds of realized composites, with remarkable R^2 values (between 0.961 and 0.983). This result is attributable to the decrease in the porosity of the specimens as the applied load increases, leading to the particles of GNPs moving closer together within the polymer matrix, consequently increasing the electrical conductivity.[53]

The results from the thermal tests are shown in Figure 8, in particular, in Figure 8A are plotted the average recorded temperatures in the whole area of the different wt% samples during the test (700 s). It can be noticed that the temperature at the end of the test for all the specimens stabilizes in an interval between 90 and 95 °C, and, in particular, samples with higher GnPs concentration within the matrix showed a higher steady state temperature. It is also worth noting that every percentage of GnPs reinforcement has a higher increase in temperature over time compared to the 0 wt% sample. Since the initial temperature is the same for all the specimens, it is possible to evaluate the temperature transient behavior for comparison. The sooner a sample reaches a certain temperature (90 °C) the better will be the thermal performance. This analysis is presented in Figure 8B, in which was considered the time to reach 90 °C of the different GnPs wt% concentration. Compared to the unreinforced specimen, all others show an improvement in the thermal performance starting from 9.5% for the 2 wt%, while for the 10 wt% sample the temperature of 90 °C is reached 33.6% sooner. This result is attributable to the presence of the dispersed GnPs through the matrix, which widely improves the thermal performance, due to its high thermal conductivity.[54]

3.3 | Tribological characterization

In this section are discussed the results of the tribological analysis of the specimens. In Figure 9A are plotted the coefficient of friction versus the sliding distance of the counterpart. It is worth noting that the coefficient of friction of the 0 wt% sample is always higher than all the GnPs reinforced ones and steading around a value after a sliding distance of 100 m of 0.52, which is typical for the PA-12.[55] The reinforced specimens show coefficient of friction values after a sliding distance of 100 m, which is steady, and starting from 0.43 for the 2 wt% to 0.38 for the 10 wt%, with a percentage improvement higher than the 25% compared to the unreinforced counterpart. Moreover, it is worth underlining that as the GnPs wt%

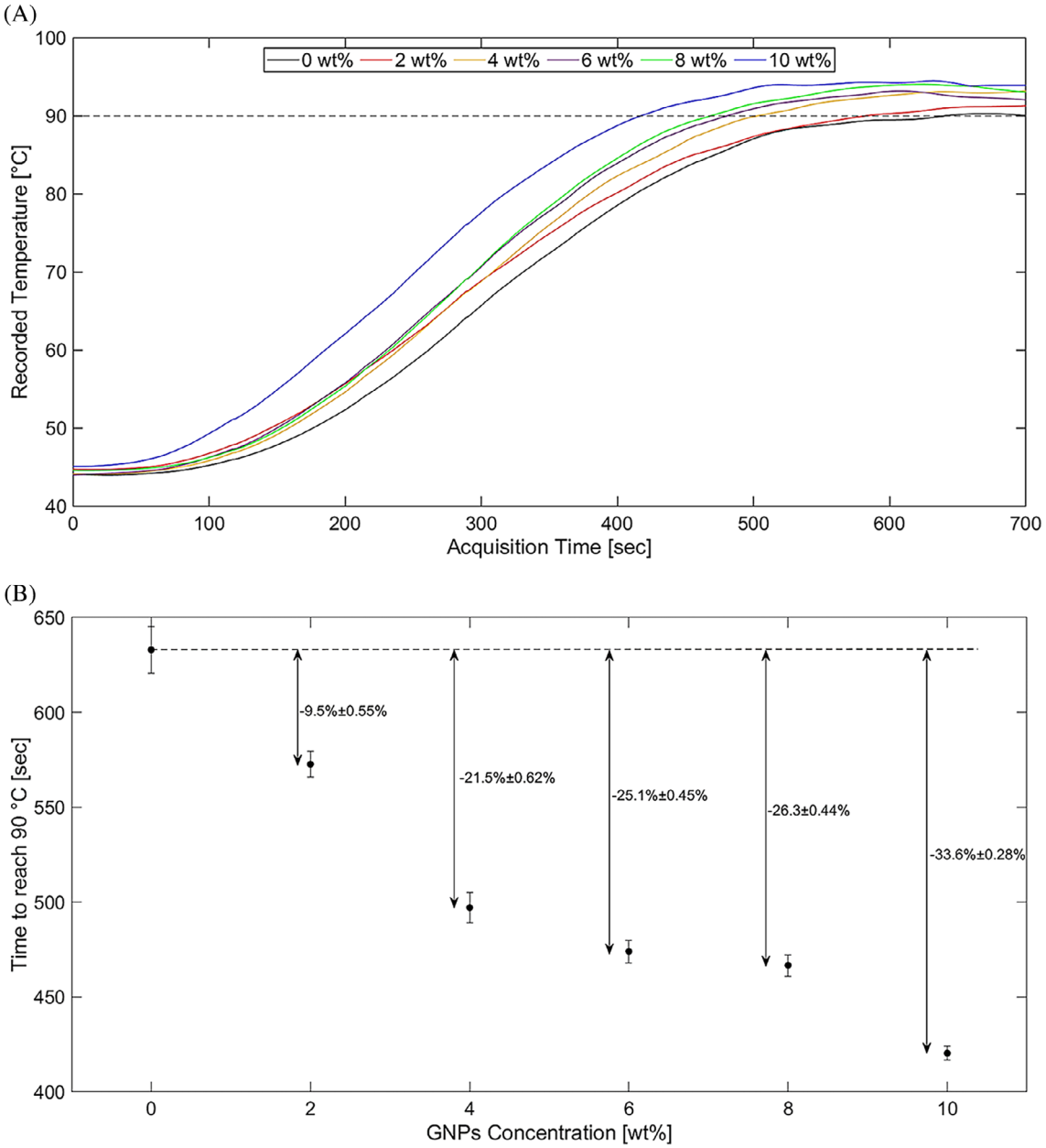

FIGURE 8 (A) Plots of recorded temperature during the test duration; (B) Time to reach 90 °C of the different wt% produced samples.

increases, it decreases the sliding distance at which the coefficient of friction value starts to be steady going from a 100 m sliding distance for the PA-12 pure sample to a 15 m sliding distance for the 10 wt% sample. Those results are attributable to the auto-lubricating properties of the GnPs, which are widely reported in the literature,[56–58] which reduces the overall friction coefficient. The more the quantity of reinforcement, the more the GnPs particles dispersed in the matrix are able to reduce the friction during the test. It is worth noting that the GnPs are well adhered within the matrix because there is no increment of the friction coefficient in the final part of the test. After the acquisition of the 3D maps of the wear traces (shown in Figure 9C), the wear volumes were calculated for each produced sample and shown in Figure 9B. The results confirm the previous ones since the wear volume decreases exponentially with the increasing of GnPs particles dispersed within the matrix. The variation starts from a value of $3.87 \cdot 10^7$ μm^3 obtained from the PA-12 pure sample to $0.73 \cdot 10^7$ μm^3 obtained for the 10 wt%, which means a percentage reduction of 81%. This decrease is undoubtedly caused by the lower tangential force acting on the sample during the test due to the lubricated contact and the notoriously excellent mechanical specific properties of the GnPs particles. The decrease of the wear volume is almost steady for the highest wt% concentrations (6-8-10 wt%),

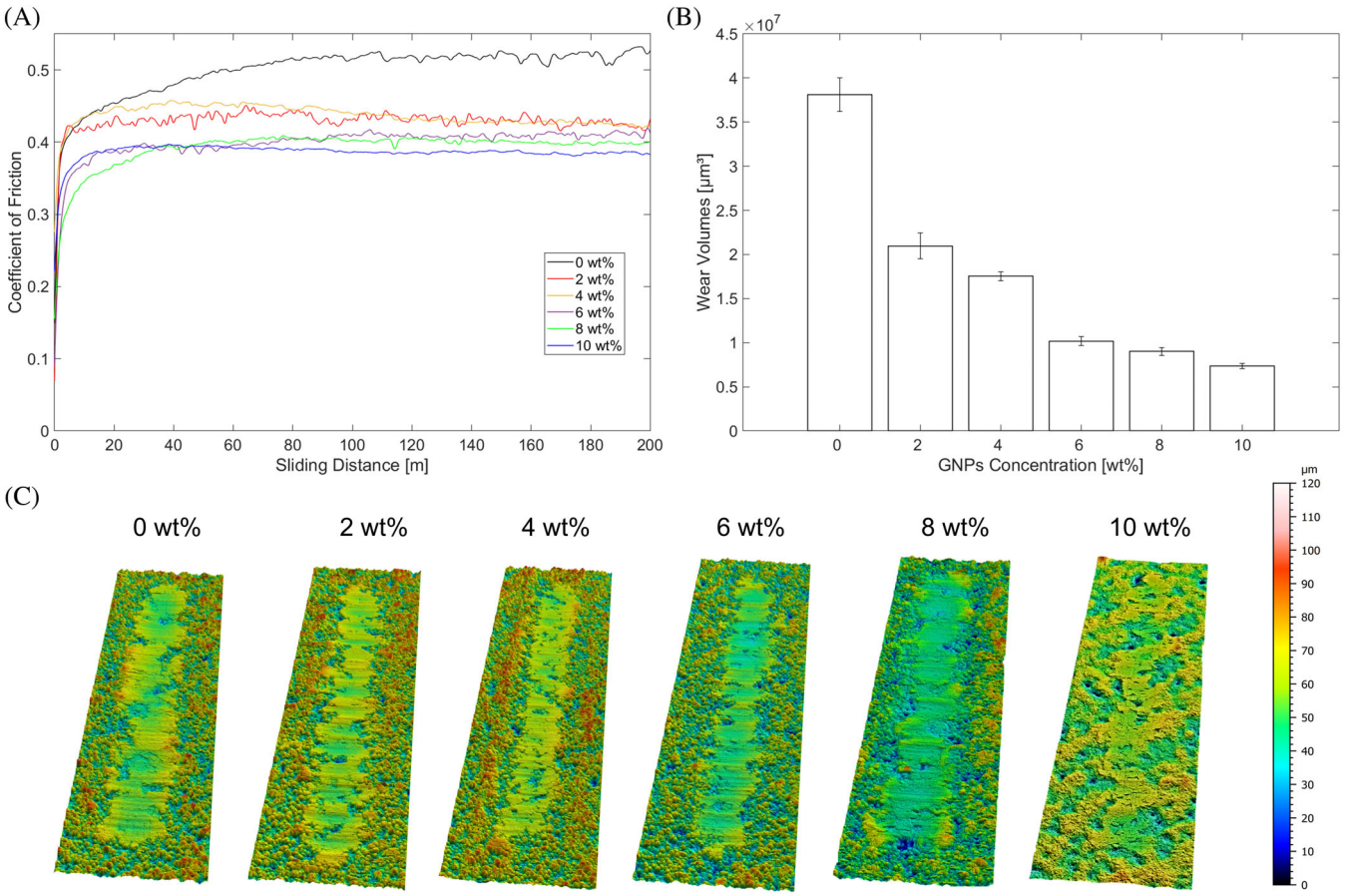

FIGURE 9 (A) Coefficient of Friction plots and (B) Calculated wear volumes of the samples with different GnPs wt% concentration; (C) Wear traces of the different GnPs wt% samples.

attributable to a balance between the increment of the porosities highlighted through the SEM analysis, and the increase in the presence of the GnPs particles on the external surface.

4 | CONCLUSIONS

Industrial-grade GnPs were successfully dispersed in polyamide (PA-12) powder through mechanical mixing and used for manufacturing components through Selective Laser Sintering (SLS) process.

It was possible to produce samples with all the wt% concentration used (2-4-6-8-10 wt%) without any significant geometrical alteration during the 3D printing process. It was also observed from the DSC analysis that the presence of the GnPs in the polymeric powder does not alter the recrystallization temperature, allowing the correct printing of the samples.

The study demonstrated that increasing GnP reinforcement within the PA-12 matrix did not significantly affect surface roughness parameters (Ra, Rz) but influenced other properties. SEM analysis revealed good adhesion and uniform dispersion of GnPs, alongside increased porosity and unsintered particles due to thermal inertia of the reinforcement. Wettability tests indicated a shift from hydrophilic to hydrophobic behavior, with up to a 43% increase in contact angle. Electrical conductivity was improved by over 8 orders of magnitude (from 10^{-11} to 10^{-4} S/cm), attributed to the conductive nature of GnPs and reduced porosity under load. Thermal performance enhanced significantly, with up to a 33.6% reduction in time to reach 90 °C. Tribological tests showed a reduction in the coefficient of friction (up to 25%) and wear volumes (up to 81%), attributed to the self-lubricating and high specific properties of the GnPs.

These findings could be of interest to researchers and engineers exploring the potential of GnP-reinforced PA-12 for industrial applications such as enclosures of electronic devices that require protection against electromagnetic interference (EMI) or the realization of 3D printed PA-12 assemblies of gears, bushings, and bearings with reduced coefficient of friction and wear.

AUTHOR CONTRIBUTIONS

All persons who meet authorship criteria are listed as authors, and all authors certify that they have participated sufficiently in the work to take public responsibility for the content, including participation in the concept, design, analysis, writing, or revision of the manuscript. Furthermore, each author certifies that this material or similar material has not been and will not be submitted to or published in any other publication before its appearance in the Journal: Polymer Composites.

ACKNOWLEDGMENTS

The authors are particularly grateful to Prof. Giacomo FALCUCCI, for the instrumentation provided that helped with the thermal characterization. Open access publishing facilitated by Universita degli Studi della Tuscia, as part of the Wiley - CRUI-CARE agreement.

CONFLICT OF INTEREST STATEMENT

The authors declare that they have no known competing financial interests or personal relationships that could have appeared to influence the work reported in this paper.

DATA AVAILABILITY STATEMENT

Data sharing not applicable to this article as no datasets were generated or analysed during the current study.

ORCID

E. Mingione https://orcid.org/0000-0002-4932-1070
D. Salvi https://orcid.org/0009-0006-6321-9204

REFERENCES

1. Lupone F, Padovano E, Ostrovskaya O, Russo A, Badini C. Innovative approach to the development of conductive hybrid composites for selective laser sintering. *Compos Part A: Appl Sci Manuf*. 2021;147:106429. doi:10.1016/j.compositesa.2021.106429
2. Yuan S, Shen F, Chua CK, Zhou K. Polymeric composites for powder-based additive manufacturing: materials and applications. *Prog Polym Sci*. 2019;91:141-168. doi:10.1016/j.progpolymsci.2018.11.001
3. Han W, Kong L, Xu M. Advances in selective laser sintering of polymers. *Int J Extreme Manuf*. 2022;4:042002. doi:10.1088/2631-7990/ac9096
4. Gueche YA, Sanchez-Ballester NM, Cailleaux S, Bataille B, Soulairol I. Selective laser sintering (SLS), a new chapter in the production of solid Oral forms (SOFs) by 3D printing. *Pharmaceutics*. 2021;13:1212. doi:10.3390/pharmaceutics13081212
5. Wu J-M, Li M, Liu S-S, Shi Y-S, Li C-H, Wang W. Selective laser sintering of porous Al_2O_3-based ceramics using both Al_2O_3 and SiO_2 poly-hollow microspheres as raw materials. *Ceram Int*. 2021;47:15313-15318. doi:10.1016/j.ceramint.2021.02.096
6. Ajdary R, Kretzschmar N, Baniasadi H, et al. Selective laser sintering of lignin-based composites. *ACS Sustain Chem Eng*. 2021;9:2727-2735. doi:10.1021/acssuschemeng.0c07996
7. Özbay B, Serhatlı E. Processing and characterization of hollow glass-filled polyamide 12 composites by selective laser sintering method. *Mater Technol*. 2022;37:213-223. doi:10.1080/10667857.2020.1824149
8. Hong R, Zhao Z, Leng J, Wu J, Zhang J. Two-step approach based on selective laser sintering for high performance carbon black/ polyamide 12 composite with 3D segregated conductive network. *Compos B Eng*. 2019;176:107214. doi:10.1016/j.compositesb.2019.107214
9. Espera AH, Valino AD, Palaganas JO, Souza L, Chen Q, Advincula RC. 3D printing of a robust Polyamide-12-carbon black composite via selective laser sintering: thermal and electrical conductivity. *Macromol Mater Eng*. 2019;304:1800718. doi:10.1002/mame.201800718
10. Meng Q, Song X, Han S, et al. Mechanical and functional properties of polyamide/graphene nanocomposite prepared by chemicals free-approach and selective laser sintering. *Compos Commun*. 2022;36:101396. doi:10.1016/j.coco.2022.101396
11. Gupta G, Rajput V, Ayachit B, et al. Sliding wear behaviour of micro-sized Kota stone dust reinforced epoxy composites using Taguchi method and Grey wolf optimisation algorithm. *Proc Inst Mech Eng C J Mech Eng Sci*. 2024;238:5724-5738. doi:10.1177/09544062231219578
12. Yang F, Zobeiry N, Mamidala R, Chen X. A review of aging, degradation, and reusability of PA12 powders in selective laser sintering additive manufacturing. *Mater Today Commun*. 2023;34:105279. doi:10.1016/j.mtcomm.2022.105279
13. Bai J, Goodridge R, Yuan S, Zhou K, Chua C, Wei J. Thermal influence of CNT on the polyamide 12 nanocomposite for selective laser sintering. *Molecules*. 2015;20:19041-19050. doi:10.3390/molecules201019041
14. Wiese M, Leiden A, Rogall C, Thiede S, Herrmann C. Modeling energy and resource use in additive manufacturing of automotive series parts with multi-jet fusion and selective laser sintering. *Procedia CIRP*. 2021;98:358-363. doi:10.1016/j.procir.2021.01.117
15. Kumar SS, Shyamala P, Pati PR, Gandla PK. Wear and frictional performance of epoxy composites reinforced with natural waste fibers and fillers for engineering applications. *Fibers Polym*. 2024;25:1429-1442. doi:10.1007/s12221-024-00519-2
16. Pati PR, Satpathy MP. Effect of process parameters on sliding wear performance of red brick dust-filled glass–epoxy composites. *Proceed Inst Mech Eng Part J: J Eng Tribol*. 2022;236:1846-1854. doi:10.1177/13506501211010553
17. Tang H, Chen H, Sun Q, Chen Z, Yan W. Experimental and computational analysis of structure-property relationship in carbon fiber reinforced polymer composites fabricated by selective laser sintering. *Compos B Eng*. 2021;204:108499. doi:10.1016/j.compositesb.2020.108499
18. Gan X, Fei G, Wang J, Wang Z, Lavorgna M, Xia H. Powder quality and electrical conductivity of selective laser sintered polymer composite components. *Structure and Properties of Additive Manufactured Polymer Components*. Elsevier; 2020:149-185. doi:10.1016/B978-0-12-819535-2.00006-5
19. Yuan Y, Hu H, Wu W, Zhao Z, Du X, Wang Z. Hybrid of multi-dimensional fillers for thermally enhanced polyamide 12 composites fabricated by selective laser sintering. *Polym Compos*. 2021;42:4105-4114. doi:10.1002/pc.26120
20. Song S, Gao Z, Lu B, Bao C, Zheng B, Wang L. Performance optimization of complicated structural SiC/Si composite ceramics prepared by selective laser sintering. *Ceram Int*. 2020;46:568-575. doi:10.1016/j.ceramint.2019.09.004

21. Özbay Kısasöz B, Serhatlı İE, Bulduk ME. Selective laser sintering manufacturing and characterization of lightweight PA 12 polymer composites with different hollow microsphere additives. *J Mater Eng Perform*. 2022;31:4049-4059. doi:10.1007/s11665-021-06481-x
22. Agrawal A, Gupta G, Pati PR, Nayak SK. Dry-sliding wear analysis and prediction using response surface method and fuzzy logic for Kota stone dust–fly ash–epoxy hybrid composites. *Proceed Inst Mech Eng Part E: J Process Mech Eng*. 2023. doi:10.1177/09544089231158902
23. Ray S, Pati PR, Gupta G, Nayak SK. Analysis and prediction of abrasion wear properties of glass–epoxy composites filled with eggshell powder. *Proceed Inst Mech Eng Part E: J Process Mech Eng*. 2022. doi:10.1177/09544089221144188
24. Yilmaz S. Comprehensive analysis of 3D printed PA6.6 and fiber-reinforced variants: revealing mechanical properties and adhesive wear behavior. *Polym Compos*. 2024;45:1446-1460. doi:10.1002/pc.27865
25. Gadelmoula A, Aldahash SA. Dry friction and Wear behavior of laser-sintered graphite/carbon fiber/polyamide 12 composite. *Polymers*. 2023;15:3916. doi:10.3390/polym15193916
26. Wang Y, Shen J, Yan M, Tian X. Poly ether ether ketone and its composite powder prepared by thermally induced phase separation for high temperature selective laser sintering. *Mater Des*. 2021;201:109510. doi:10.1016/j.matdes.2021.109510
27. Yuan S, Zheng Y, Chua CK, Yan Q, Zhou K. Electrical and thermal conductivities of MWCNT/polymer composites fabricated by selective laser sintering. *Compos Part A: Appl Sci Manuf*. 2018;105:203-213. doi:10.1016/j.compositesa.2017.11.007
28. Santo J, Penumakala PK. Influence of processing techniques on mechanical and electrical performance of PLA-graphene composite feedstock filaments. *J Manuf Process*. 2023;108:513-528. doi:10.1016/J.JMAPRO.2023.11.021
29. Safian MT, Umar K, Mohamad Ibrahim MN. Synthesis and scalability of graphene and its derivatives: a journey towards sustainable and commercial material. *J Clean Prod*. 2021;318:128603. doi:10.1016/j.jclepro.2021.128603
30. Lopes AC, Sampaio ÁM, Pontes AJ. Development and characterization of composite materials with multi-walled carbon nanotubes and graphene nanoplatelets for powder bed fusion. *Rapid Prototyp J*. 2024;30:95-105. doi:10.1108/RPJ-04-2023-0142
31. Badini C, Padovano E, De Camillis R, Lambertini VG, Pietroluongo M. Preferred orientation of chopped fibers in polymer-based composites processed by selective laser sintering and fused deposition modeling: effects on mechanical properties. *J Appl Polym Sci*. 2020;137:49152. doi:10.1002/app.49152
32. Khudiakova A, Berer M, Niedermair S, et al. Systematic analysis of the mechanical anisotropy of fibre-reinforced polymer specimens produced by laser sintering. *Addit Manuf*. 2020;36:101671. doi:10.1016/j.addma.2020.101671
33. Chen B, Davies R, Liu Y, et al. Laser sintering of graphene nanoplatelets encapsulated polyamide powders. *Addit Manuf*. 2020;35:101363. doi:10.1016/j.addma.2020.101363
34. Rietzel D, Aquite W, Drummer D, Osswald T. Polymer powders for selective laser sintering – production and characterization. *Proc. 44th CIRP Conference on Manufacturing Systems*; Madison, WI, US. 2011:1-6.
35. Amado A, Schmid M, Levy G, Wegener K. Advances in SLS powder characterization. Proceedings 22nd Annual International Solid Freeform Fabrication Symposium - An Additive Manufacturing Conference; University of Texas at Austin; 2011:438-452. doi:10.26153/tsw/15306
36. Amankwah NYA, Agbenorhevi JK, Rockson MAD. Physicochemical and functional properties of wheat-rain tree (Samanea saman) pod composite flours. *Int J Food Prop*. 2022;25:1317-1327. doi:10.1080/10942912.2022.2077367
37. Hong G, Han Y, Schutzius TM, et al. On the mechanism of hydrophilicity of graphene. *Nano Lett*. 2016;16:4447-4453. doi:10.1021/acs.nanolett.6b01594
38. Almonti D, Baiocco G, Della MM, et al. Morphological and functional characterization of electroplated Ni-graphene composite coatings. *J Phys Conf Ser*. 2024;2692:012008. doi:10.1088/1742-6596/2692/1/012008
39. Jia B-B, Li T-S, Liu X-J, Cong P-H. Tribological behaviors of several polymer–polymer sliding combinations under dry friction and oil-lubricated conditions. *Wear*. 2007;262:1353-1359. doi:10.1016/j.wear.2007.01.011
40. Li X, Zhang R, Hung WST, Olofsson U, Manuel L, Duan C. A pin-on-disk study of the tribological properties of polyoxymethylene (POM) gear materials. *IEEE Trans Instrum Meas*. 2024;73:1-10. doi:10.1109/TIM.2024.3400329
41. Lim S, Park H, Yamamoto G, Lee C, Suk JW. Measurements of the electrical conductivity of monolayer graphene flakes using conductive atomic force microscopy. *Nanomaterials*. 2021;11:2575. doi:10.3390/nano11102575
42. Shtein M, Nadiv R, Buzaglo M, Kahil K, Regev O. Thermally conductive graphene-polymer composites: size, percolation, and synergy effects. *Chem Mater*. 2015;27:2100-2106. doi:10.1021/cm504550e
43. Hejmady P, van Breemen LCA, Hermida-Merino D, Anderson PD, Cardinaels R. Laser sintering of PA12 particles studied by in-situ optical, thermal and X-ray characterization. *Addit Manuf*. 2022;52:102624. doi:10.1016/j.addma.2022.102624
44. Barbosa-Cánovas GV, Ortega-Rivas E, Juliano P, Yan H. *Food Powders*. 1st ed. Springer US; 2005. doi:10.1007/0-387-27613-0
45. Alshammari BA, Al-Mubaddel FS, Karim MR, Hossain M, Al-Mutairi AS, Wilkinson AN. Addition of graphite filler to enhance electrical, morphological, thermal, and mechanical properties in poly (ethylene terephthalate): experimental characterization and material modeling. *Polymers*. 2019;11:1411. doi:10.3390/polym11091411
46. Ferreira CI, Dal Castel C, Oviedo MAS, Mauler RS. Isothermal and non-isothermal crystallization kinetics of polypropylene/exfoliated graphite nanocomposites. *Thermochim Acta*. 2013;553:40-48. doi:10.1016/j.tca.2012.11.025
47. Liu F, Wang M, Chen Y, Gao J. Thermal stability of graphene in inert atmosphere at high temperature. *J Solid State Chem*. 2019;276:100-103. doi:10.1016/j.jssc.2019.04.008
48. Cilento F, Claudio L, Genna S, Giordano M, Martone A. Graphene NanoPlatelet-based coating as thermal protection from high-power radiative fluxes. *Compos Struct*. 2023;319:117157. doi:10.1016/j.compstruct.2023.117157
49. Ashok Kumar SS, Bashir S, Ramesh K, Ramesh S. A comprehensive review: super hydrophobic graphene nanocomposite coatings for underwater and wet applications to enhance

corrosion resistance. *FlatChem*. 2022;31:100326. doi:10.1016/j.flatc.2021.100326

50. Pearson GL, Bardeen J. Electrical properties of pure silicon and silicon alloys containing boron and phosphorus. *Phys Rev*. 1949;75:865-883. doi:10.1103/PhysRev.75.865
51. Morita N, Yamamoto A. Optical and electrical properties of boron. *Jpn J Appl Phys*. 1975;14:825-832. doi:10.1143/JJAP.14.825
52. Putley EH. The electrical conductivity of germanium. *Proceed Phys Soc Section A*. 1949;62:284-292. doi:10.1088/0370-1298/62/5/303
53. Govorov A, Wentzel D, Miller S, Kanaan A, Sevostianov I. Electrical conductivity of epoxy-graphene and epoxy-carbon nanofibers composites subjected to compressive loading. *Int J Eng Sci*. 2018;123:174-180. doi:10.1016/j.ijengsci.2017.11.014
54. Mahanta NK, Abramson AR. Thermal conductivity of graphene and graphene oxide nanoplatelets. *13th InterSociety Conference on Thermal and Thermomechanical Phenomena in Electronic Systems*. IEEE; 2012:1-6. doi:10.1109/ITHERM.2012.6231405
55. Wörz A, Drummer D. Tribological anisotropy of selective laser sintered PA12 parts. *Polym Test*. 2018;70:117-126. doi:10.1016/j.polymertesting.2018.06.028
56. Almonti D, Baiocco G, Menna E, Mingione E, Rubino G, Ucciardello N. Characterisation of Cu-GnP composite coatings for friction control and wear resistance applications. *Eng Fail Anal*. 2022;139:106419. doi:10.1016/j.engfailanal.2022.106419
57. Baiocco G, Menna E, Salvi D, Ucciardello N. Investigating tribological properties of electrophoretically deposited graphene nanoplatelets coatings on mild steel. *Thin Solid Films*. 2024;793:140279. doi:10.1016/j.tsf.2024.140279
58. Baiocco G, Genna S, Salvi D, Ucciardello N. Laser texturing to increase the Wear resistance of an electrophoretic graphene coating on copper substrates. *Materials*. 2023;16:5359. doi:10.3390/ma16155359

SUPPORTING INFORMATION

Additional supporting information can be found online in the Supporting Information section at the end of this article.

How to cite this article: Mingione E, Salvi D, Almonti D, Ponticelli GS. Improvement of thermal, electrical, and tribological performances of GnPs composites produced by selective laser sintering. *Polym Compos*. 2025;1-15. doi:10.1002/pc.29467